Fractional anisotropy as a tracer of cosmic voids

Sebastian Bustamante [*1], Jaime E. Forero-Romero[2]

[1]*Instituto de Física - FCEN, Universidad de Antioquia, Calle 67 No. 53-108, Medellín, Colombia*
[2]*Departamento de Física, Universidad de los Andes, Cra. 1 No. 18A-10, Edificio Ip, Bogotá, Colombia*

4 September 2014

ABSTRACT
In the last decades voids have been identified as one of the most important features of the Megaparsec Universe, therefore a full understanding of their properties is required in order to a proper description of the large-scale structure of the Cosmic Web. Identifying voids in cosmological observations (e.g. redshift galaxy surveys) and N-body simulations is hence an important enterprise that must be carried out and accordingly, a plethora of different void finding techniques can be found in the literature.

We present here a novel approximation for finding voids in cosmological simulations based upon two different schemes commonly used for quantifying the Cosmic Web, i.e. the T-web and the V-web (the so-called web schemes), which have proven to be very adequate for that purpose. Unlike previously defined void finding techniques based on the density field, we use here the fractional anisotropy (FA) computed from the eigenvalues of each web scheme and then, through a Watershed Transform, we identify individual voids as the catching basins of local minima of the FA field. Like other Watershed Transform-based schemes, ours retains the same advantages, i.e., it is relatively free-parameter and makes no significant assumptions on the shape and structure of voids.

We test our method on the Bolshoi simulation and compare with a density-based scheme. We find our method gives a better resemblance of the visual impression of the distribution of voids within the Cosmic Web, in addition to a more robust description of voids as it allows to identify, in a very clear manner, their outlines as regions where the FA is maximized, normally corresponding to walls and filaments. This is mainly because of the non-monotonic behaviour of the FA, what allows to use it as a sort of one-dimensional tomography of the Cosmic Web.

Key words: Cosmology: theory - large-scale structure of Universe - Methods: data analysis - numerical - N-body simulations

1 INTRODUCTION

Since voids where discovered in the first compiled galaxy surveys (Chincarini & Rood 1975; Gregory & Thompson 1978; Einasto et al. 1980a,b; Kirshner et al. 1981, 1987), they have been identified, along with the filamentary and hierarchically clustered nature of the Cosmic Web, as one of the most striking features of the Megaparsec Universe (Bond et al. 1996). Nevertheless, due to the large volume extension of void regions ($\sim 5 - 10$ Mpch^{-1}), statistically meaningful catalogues of voids (Pan et al. 2012; Sutter et al. 2012; Nadathur & Hotchkiss 2014) only have become available after modern large galaxy surveys like the two-degree field Galaxy Redshift Survey (Colless et al. 2001, 2003) and the Sloan Digital Sky Survey (York et al. 2000; Abaza-

jian et al. 2003), thereby triggering a plethora of more refined observational and statistical studies of voids throughout the last decade (Hoyle & Vogeley 2004; Croton & et al. 2004; Rojas et al. 2005; Ceccarelli et al. 2006; Patiri et al. 2006; Tikhonov 2006; Patiri et al. 2006; Tikhonov 2007; von Benda-Beckmann & Müller 2008; Foster & Nelson 2009; Ceccarelli et al. 2013; Sutter et al. 2014)

On the theoretical side, early descriptions of the evolution of the large-scale Universe, based on gravitational instabilities in primordial stages and leaded by the seminal work of Zel'dovich (1970), are consistent with the Cosmic Web picture, where planar pancake-like regions of matter enclose enormous underdense voids and are bordered, in turn, by thin filaments and high-density clumpy knots (Bond et al. 1996). First theoretical models for describing formation, dynamics and properties of voids (Hoffman & Shaham 1982; Icke 1984; Bertschinger 1985; Blumenthal et al. 1992)

were dramatically complemented and extended by first numerical studies based on simulations (Martel & Wasserman 1990; Regos & Geller 1991; van de Weygaert & van Kampen 1993; Dubinski et al. 1993). This tendency of using numerical data from N-body simulations, fuelled by last generation computing systems and ever more efficient numerical algorithms, has become increasingly common in the last years as a powerful analysis toolkit of cosmic voids (for an extensive compilation of previous numerical works, see Colberg et al. (2008)).

At present, studying voids may be considered as a threefold enterprise (Platen et al. 2007): first, they are a key ingredient of the Cosmic Web as they dominate almost the entire volume distribution at large-scales and additionally, they compensate overdense structures in the total budget of matter. This implies that a full understanding of their evolution and properties is essential for fathoming the high complexity of the Cosmic Web. Second, they provide a valuable resource for inferring and probing cosmological parameters as their structure and dynamics are highly determined by these values. Third, they constitute and unique and still largely pristine environment in which can be tested galaxy evolution.

Although a visual recognition of voids in galaxy surveys and simulations is possible in most cases, a formal systematic identification is necessary for statistically meaningful studies. However, a basic yet essential issue remains regarding the definition itself of what a void is. There is not a general consensus about an unambiguous definition of cosmic voids and therefore, there can be found many different void finding techniques throughout the literature (for a detailed comparison of different schemes, see the Void Finder Comparison Project Colberg et al. (2008)). In spite of the diversity of existing schemes, they can be roughly classified into two main types: first, geometric schemes based on point spatial or redshift distribution of galaxies in surveys or catalogues of dark matter halos in simulations (Kauffmann & Fairall 1991; Müller et al. 2000; Gottlöber et al. 2003; Hoyle & Vogeley 2004; Brunino et al. 2007; Foster & Nelson 2009; Micheletti & et al. 2014; Sutter et al. 2014), and second, schemes based on the smooth and continuous matter density field either from simulations or from reconstruction procedures on surveys (Plionis & Basilakos 2002; Colberg et al. 2005; Shandarin et al. 2006; Platen et al. 2007; Neyrinck 2008; Neyrinck et al. 2013; Ricciardelli et al. 2013).

Here we introduce a new tracer of the structure of cosmic voids built from two tensorial web schemes, i.e. the T-web, based on the Hessian of the gravitational potential or tidal tensor (Hahn et al. 2007; Forero-Romero et al. 2009), and the V-web, based on the velocity shear tensor (Hoffman et al. 2012). These web schemes classify the Cosmic Web into four different types of environment depending on the counting of the number of eigenvalues below an user-defined threshold (λ_{th}), namely voids (3 eigenvalues below λ_{th}), sheets (2), filaments (1) and knots or clusters (0). The tidal and the shear tensors have proven to be more fundamental than the density field as they also trace the collapsing or expanding nature of the matter field, which ultimately is what defines the underlying dynamics of the Cosmic Web. Furthermore, the density field is degenerated regarding the defined types of environment (Hahn et al. 2007), which implies that is not possible to assign a priori a range of density

values to each of them. This yields that the usually adopted definition of voids as simply underdense regions in the large-scale matter distribution, is not precise enough as it excludes a proper description of the internal structure of voids.

Following the recent trend of using digital image-processing techniques developed in other disciplines (e.g. medical sciences and computer imaging) for analysing the structure of the Cosmic Web, we propose here, much in the same way as Libeskind et al. (2013), the fractional anisotropy (FA) as a tracer of the internal structure and the outline of cosmic voids. The FA was initially introduced by Basser (1995) for quantifying the anisotropy degree of the diffusivity of water molecules through cerebral tissue in nuclear magnetic resonance imaging. In this context we use the same quantity for determining the anisotropy degree of the local environment from either the orbital dynamics as set by the eigenvalues of the tidal tensor (T-web), or the dynamics of the velocity field as set by the eigenvalues of the shear tensor (V-web). In both cases, the FA is not determined directly from the density field, hence it is suitable for describing both, the structure of high non-linear regions (e.g. filaments, knots and very dense walls) as well as for revealing the fainter substructure exhibited by quasi-linear regions like voids.

Once established the FA as the tracer field of cosmic voids, we proceed to identify individual voids as basins of local minima. For this purpose we implement a technique defined by Beucher & Lantuejoul (1979) and Beucher & Meyer (1993) and widely used in the field of image analysis and mathematical morphology, i.e. the *watershed transform algorithm*. This technique has been already implemented on void finding schemes by Platen et al. (2007) and Neyrinck (2008) with very interesting results, where individual voids are identified as catching basins of local minima of the density field. The appeal of this algorithm lies in that is parameter-free and does not require to make any assumption on the shape and morphology of voids. Although we use a *cloud-in-cell* (`CIC`) algorithm on a Cartesian mesh for estimating the density and tensor fields, instead of the more sophisticated *Delaunay tessellation for field estimator* (`DTFE`) technique (Schaap & van de Weygaert 2000), our implementation of the watershed transform should not be significantly affected as we are interested in quasi-linear regions where the `CIC` gives similar estimations.

This paper is organized as follows. In section 2 we describe the used simulation for testing our void finding algorithm, i.e. the Bolshoi simulation. Alternatively to the web schemes T-web and V-web, we propose a very basic web classifier based on three threshold values defined on the density field, this is used in our comparisons as a representative of all density-based schemes. A detailed description of these schemes is presented in section 3. In section 4 we describe how the FA can be used for tracing the structure of voids. Once obtained meaningful catalogues of voids for each scheme, we proceed to compare some typical and general interest properties of voids such as volume functions, distributions of size and density and velocity profiles. This is done in section 5. Finally in section 6 we analyse and evaluate our findings.

2 THE SIMULATION

We use here an unconstrained cosmological simulation (the Bolshoi simulation) to identify the possible large scale environment and the distribution of cosmic voids at $z = 0$. The Bolshoi simulation follows the non-linear evolution of a dark matter density field on a cubic volume of size $250h^{-1}\mathrm{Mpc}$ sampled with 2048^3 particles. The cosmological parameters in the simulation are $\Omega_\mathrm{m} = 0.27$, $\Omega_\Lambda = 0.73$, $h = 0.70$, $n = 0.95$ and $\sigma_8 = 0.82$ for the matter density, cosmological constant, dimensionless Hubble parameter, spectral index of primordial density perturbations and normalization for the power spectrum respectively, consistent with the seventh year of data of the Wilkinson Microwave Anisotropy Probe (WMAP) (Jarosik et al. 2011). For more detailed technical information about the simulation, see Klypin et al. (2011).

With the above parameters the mass of each particle in the simulation is $m_\mathrm{p} = 1.4 \times 10^8 h^{-1}\mathrm{M}_\odot$. Throughout this paper we shall use a catalogue of halos identified through the Bound Density Maximum algorithm (Klypin et al. 1999). These halos have been selected to have an overdensity of 200 times the critical density in addition to be mutually excluded of the virial radius of other halos. Mass, comoving position and peculiar velocity of each halo at $z = 0$ were obtained through the public available Multidark database [1] (Riebe et al. 2011). For estimating the density and velocity fields we use a *cloud-in-cell* (`CIC`) algorithm onto a grid of 256^3 cells, corresponding to a resolution of $0.98h^{-1}\mathrm{Mpc}$ per cell side. Then, through finite-differences and FFT methods the tidal and shear tensors are computed. Finally the eigenvalues and eigenvectors of each tensor are obtained for each cell of the grid. Neglecting substructures presented below Megaparsec scales and taking into account our focus in voids, which are a prominent characteristic of the Megaparsec Universe, we apply a Gaussian softening of one cell to all fields.

3 ALGORITHMS TO QUANTIFY THE COSMIC WEB

3.1 The tidal web (T-web)

This scheme was initially proposed by Hahn et al. (2007) as a novel alternative for classifying the Cosmic Web based on the tidal tensor, that is somehow more fundamental than the density field as it also allows to quantify the orbital dynamics of the matter field. This approach is reached by a second-order expansion of the equations of motion around local minima of the gravitational potential and then extended to any position. The second-order term corresponds to the tidal tensor, which is defined as the Hessian of the normalized gravitational potential

$$T_{\alpha\beta} = \frac{\partial^2 \phi}{\partial x_\alpha \partial x_\beta} \qquad (1)$$

where the physical gravitational potential has been rescaled by a factor $4\pi G\bar\rho$ in such a way that ϕ satisfies the following equation

$$\nabla^2 \phi = \delta, \qquad (2)$$

with $\bar\rho$ the average density in the Universe, G the gravitational constant and δ the dimensionless matter overdensity.

Since the tidal tensor can be represented in any cell by a real and symmetric 3×3 matrix, it is ensured the possibility to diagonalize it and obtain three real eigenvalues $\lambda_1 \geqslant \lambda_2 \geqslant \lambda_3$. This set of eigenvalues can be used as indicators of the local orbital stability in each proper direction, which in turn can be translated into a classification scheme of the Cosmic Web. A counting of the number of positive (stable) or negative (unstable) eigenvalues allows to catalogue a single cell into one of the next four types of environment: voids (3 negatives eigenvalues), sheets (2), filaments (1) and knots (0). A significant improvement to this scheme was introduced by Forero-Romero et al. (2009) by means of a relaxation of the stability criterion. The relative strength of each eigenvalue is no longer defined by the sign, but instead by a threshold value λ_{th} that can be tuned in such a way that the visual impression of the web-like matter distribution is reproduced.

3.2 The velocity web (V-web)

We also use a kinematical scheme to define the Cosmic Web environment in the simulation. The scheme has been thoroughly described in Hoffman et al. (2012) and applied to study the shape and spin alignment in the Bolshoi simulation in Libeskind et al. (2013). We refer the reader to these papers to find a detailed description of the algorithm, its limitations and capabilities. The V-web scheme for environment finding is based on the local velocity shear tensor calculated from the smoothed dark matter velocity field in the simulation. The central quantity is given by the following dimensionless expression

$$\Sigma_{\alpha\beta} = -\frac{1}{2H_0}\left(\frac{\partial v_\alpha}{\partial x_\beta} + \frac{\partial v_\beta}{\partial x_\alpha}\right) \qquad (3)$$

where v_α and x_α represent the α component of the comoving velocity and position, respectively. Like the tidal tensor, $\Sigma_{\alpha\beta}$ can be represented by a 3×3 symmetric matrix with real values, hence diagonalizing it is obtained three real eigenvalues $\lambda_1 \geqslant \lambda_2 \geqslant \lambda_3$ whose sum (the trace of $\Sigma_{\alpha\beta}$) is proportional to the divergence of the local velocity field smoothed on the physical scale $\mathcal{R}$.

In the same way, the relative strength of the three eigenvalues with respect to a threshold value λ_{th} allows for the local classification of the matter distribution into the previous four web types. For the threshold choosing in both schemes, the V-web and the T-web, it is usual to fine-tuning the value in such a way that the visual appearance of the Cosmic Web as seen in simulations and galaxy surveys is reproduced. However, we do not take this approach here, instead we propose a novel approach for the threshold choosing based on the maximization of the fractional anisotropy field occurring in filaments and very dense walls.
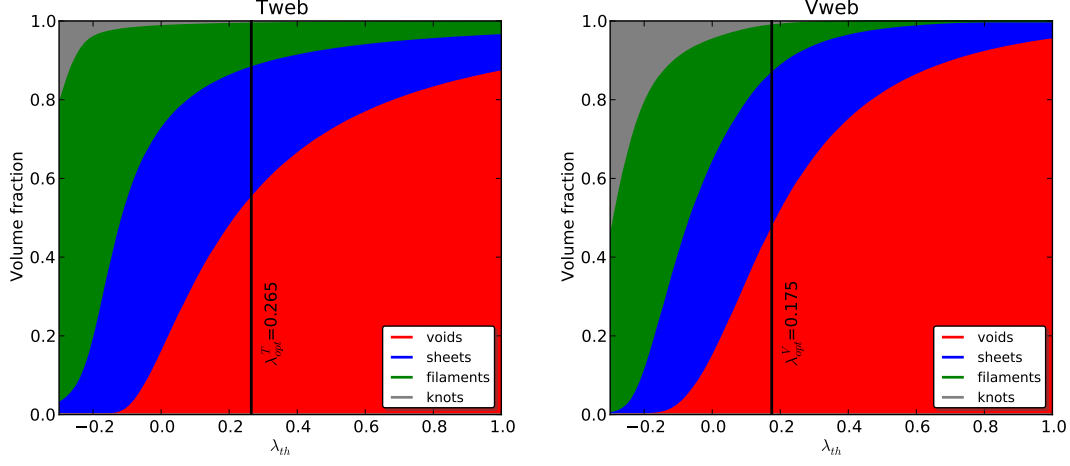
---

[1] `http://www.multidark.org/MultiDark/`

Figure 1. Volume Filling Fraction for each type of environment with respect to the chosen threshold λ_{th} for both web schemes (T-web, left panel. V-web, right panel). For each case, the threshold value is chosen such that the fractional anisotropy along the void-sheet boundaries has a value of $FA = 0.95$.
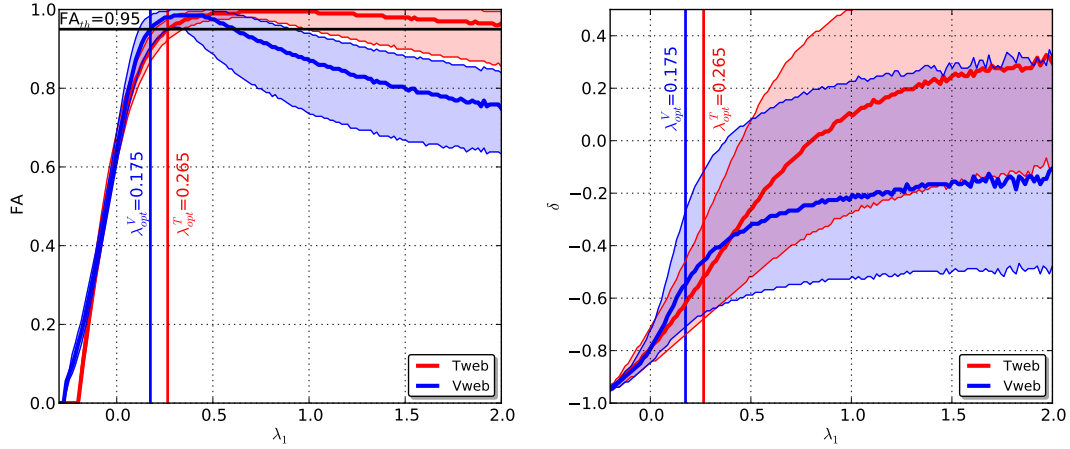

Figure 2. Distributions of fractional anisotropy (left panel) and density field (right panel) with respect to the eigenvalue λ_1 for each web scheme (T-web, red lines. V-web, blue lines) as calculated over all cells of the grid. Thick central lines correspond to the median and filled regions to the 50% of the distribution.

3.3   The density-based web finder

Although the density field is a key quantity for understanding the large-scale Universe, the filamentary structure of the Cosmic Web is poorly traced by it (see e.g. figure 3). In order to compare our new proposal based on the the fractional anisotropy as a tracer field of voids, we define a very basic approach for environmental finding based on three thresholds of the density field.

In next section we shall describe an alternative approximation to select the threshold value λ_{th}, and as will be shown, one of its main advantages is the similar volume filling fraction (VFF) of each environment as compared between both web schemes. Using this result, we propose here a heuristic classification of the Cosmic Web based on three density thresholds assigned to each boundary (i.e. void-sheet, sheet-filament and filament-knot)[2] such that the cor-

Volume Filling Fraction	Scheme			Threshold
	T-web	**V-web**	**Density**	$\delta_{\mathbf{th}}$
Voids	54.88%	47.06%	50.97%	-0.57
Sheets	33.21%	39.54%	36.38%	0.60
Filaments	11.16%	12.18%	11.67%	8.82
Knots	0.75%	1.22%	0.98%	$-$

Table 1: VFF for each type of environment and for each web scheme. VFF for the density-based scheme are defined as the arithmetic mean of the T-web and the V-web. The last column corresponds to the threshold values in the density field in order to obtain the required VFF. Note there is not any value associated to knots as there is not a higher order environment.

---

[2] The progressive sequence void-sheet-filament-knot along any path in the Cosmic Web should be always satisfied as each used

field is smoothed. For instance, it should not be possible to find a knot-type cell abutting another sheet or void-type cell.
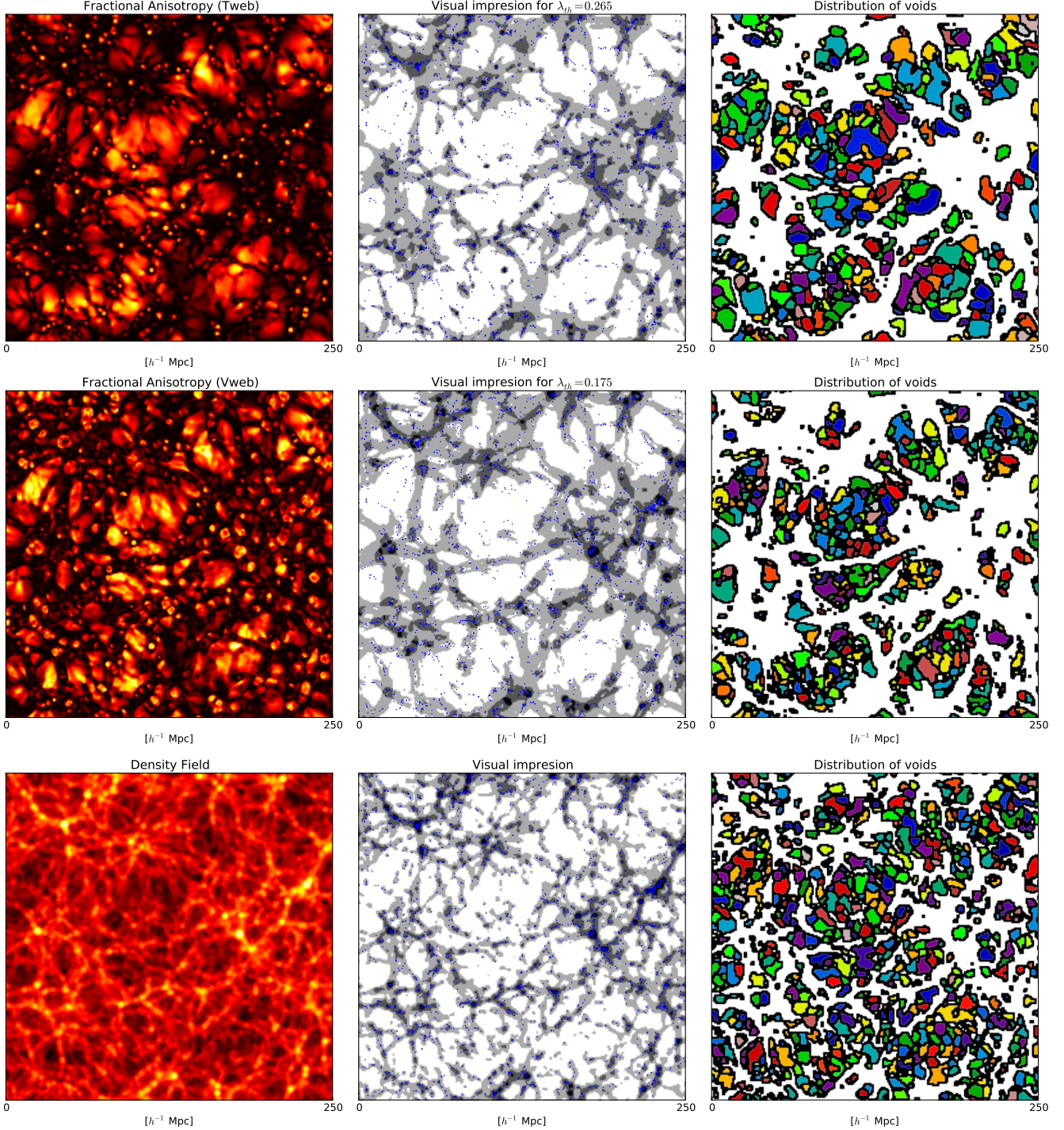
Figure 3. Left panels show the visual impression of the Cosmic Web for each web scheme (T-web, upper panels. V-web, middle panels. Density, lower panels). It can be noticed each environment sketched such that voids corresponds to white, sheets to gray, filaments to dark gray and knots to black regions. Right panels show the fractional anisotropy field for the same slide of the simulation and for each web scheme. Black regions correspond to the maxim value, i.e. FA= 1, while white and light yellow regions to FA= 0. It is worth noting the degeneration of low values of FA for knots and central regions of voids, thus indicating a high isotropy for both processes. In the same way, high values of FA (FA $\lesssim$ 1) are consistent the anisotropic geometry exhibited by filaments and very flat sheets.

responding VFF values are similar to the values obtained for the T-web and the V-web, specifically they are defined to be the arithmetic mean of both schemes.

4   FINDING BULK VOIDS

4.1   Fractional anisotropy as tracer of voids

According to the recent growing interest in studying galaxy formation in low-density regions as cosmological tests, classifying void regions is becoming an important task in cosmology. Most of those classification schemes for voids in cosmological simulations are based upon the density field, setting a cut off value below which some region becomes a void [**references**]. Some more advanced classification schemes are based on Voronoi tessellations applied over the tracer particles of the simulation in order to compute the density field. Then, through a watershed transform, a hierarchy of void regions are found [**references, ZOBOV algorithm**].

As has been established [**references**], both web schemes presented in the previous section (V-web and T-web) for classifying the cosmic web present many advantages compared with classification schemes based completely upon the density field, e.g. a more robust description of the dynamic a kinematic of the cosmic web, a more reliable quantification of the visual impression, among others. With the aim of exploiting all of these advantages, we propose here a novel approach to classify voids in cosmological simulations based entirely on the web schemes.

The original version of the T-web scheme [**reference, Hahn**] was not successful at reproducing the visual impression of the cosmic web, however, with the introduction of a threshold parameter [**reference, Forero-Romero**], this scheme, and even the V-web [**reference, Hoffman**], improved enormously. As this free parameter controls the visual impression provided by each scheme, phenomenons like percolation depends on it as well. Although percolation is one of the key features of the structure of void regions, indicating how voids are merged among them, and how they permeate all the cosmic web, our primal interest here is studying properties of single voids. Nevertheless, in the next section we shall analyse briefly the percolation phenomenon for both web schemes.

In order to deal with percolation of voids in our classification scheme, we introduce the fractional anisotropy as defined in [**reference, Libeskind**].

$$FA = \frac{1}{\sqrt{3}} \sqrt{\frac{(\lambda_1 - \lambda_3)^2 + (\lambda_2 - \lambda_3)^2 + (\lambda_1 - \lambda_2)^2}{\lambda_1^2 + \lambda_2^2 + \lambda_3^2}} \quad (4)$$

where the eigenvalues are taken from any of the two web schemes. This index, such as it is defined, allows quantifying the local anisotropy degree of the cosmological environment, where $FA = 0$ corresponds to highly isotropic regions and $FA = 1$ anisotropic ones.

In the figure 3 we calculate the FA field over the simulation for both web schemes. The first interesting feature of this figure is the degeneration presented for knots and central regions of voids, where both of them exhibit low to middle values of the FA, indicating a high isotropy regarding the physical properties quantified by each web scheme, i.e. the

density field for the T-web and the peculiar velocity for the V-web. For the T-web, the FA field near to knots presents a very narrow distribution around a local minimum, whereas for the V-web such distribution is more spread out. This can be explained appealing to the low fluctuations of the density field compared with the peculiar velocity in highly non-linear regions like knots. For more linear regions like voids, the behaviour of the FA field is quite similar between both schemes, what is consistent with the equivalence of the T-web and the V-web in the linear regime [**reference, Hoffman**].

According to the classification scheme adopted for the cosmological environment, voids are regions where $\lambda_3 \leqslant \lambda_2 \leqslant \lambda_1 \leqslant \lambda_{th}$. This implies that the boundaries of void regions are controlled completely by the λ_1 eigenvalue of the web scheme and the threshold value. Therefore, as we increase the threshold value λ_{th}, all voids grow up progressively through contours of the λ_1 field until certain critical value where they are so large that the visual impression is no longer reproduced. Our objective here is to find a reliable quantity that allows to trace the geometry of void regions as classified by each web scheme. In the figure 2 we calculate the distributions of the fractional anisotropy index and the density field regarding the λ_1 eigenvalue for both web schemes over all the cells of the simulation. Thick lines correspond to the median of the distributions, whereas coloured regions correspond to 50% of the sample, delimited by quartiles Q_1 and Q_3.

The first important conclusion is regarding the distribution of the FA index, where there is an almost perfect correlation with the λ_1 eigenvalue for low values of it. This result can be interpreted as an one-dimensional tomography of void regions, where low λ_1 values are associated to the central regions of voids, these being the most isotropic structures found, with FA values close to 0. As we increase the λ_1 value, corresponding to progressively outer layers of void regions or less isotropic voids, the FA index increases as well, maintaining a very reliable correlation approximately until $FA = 0.95$. This limit value of the FA can be traduced in terms of an optimal λ_{th}, where we obtain $\lambda_{opt}^V = 0.175$ for the V-web scheme and $\lambda_{opt}^T = 0.265$ for the T-web scheme, both values consistent with optimal thresholds normally taken in previous works [**references**]. Due to the definition of the fractional anisotropy index, it presents the highest values for filaments and very flat sheets, i.e. $FA \lesssim 1$. Therefore, if we extend the λ_{th} value beyond the optimal FA limit, such that the outer regions of voids becomes highly anisotropic, it would imply that voids are invading filaments and sheets, so the optimal λ_{th} value is a limit value up to which we can have void regions. For other type of environment such as sheets, filaments and knots, the λ_1 eigenvalue does not control their spatial boundaries, so the correlation with the FA index is no longer valid beyond the threshold values, furthermore the larger dispersion of the FA distribution also indicates that contours of the FA field are no longer corresponding to contours of the λ_1 field. Nevertheless, for high λ_1 values, i.e. $\lambda_1 > 1.0$, the median value of the FA index decreases to lower values, indicating the presence of isotropic knots. All of this allows us to conclude that the distribution of the FA with respect to the λ_1 eigenvalue is not only an one-dimensional tomography of voids, but also a sort of one-dimensional projection of the global structure

of the cosmic web, starting in highly isotropic central voids, passing through very anisotropic sheets and filaments, until isotropic knot regions.

For the distribution of the density with respect to the λ_1 eigenvalue, it can be appreciated an analogous behaviour, where central regions of voids present the most underdense values of the overall cosmic web. For outer layers of voids, the density field grows progressively until sheets and filaments are reached. However, the dispersion in the distributions indicates that the geometry of voids as quantified by both web schemes is not compatible with the density field, i.e. contours of the λ_1 eigenvalue do not coincide with contours of the density field. Then, the density is not a reliable quantity to be used as tracer of our voids. Furthermore, another advantage of using the FA index instead of the density is the non-monotonous behaviour of the FA median value, with a local maxima that allows to identify properly the boundaries of voids.

4.2 Identifying void regions through web schemes

Resuming our endeavour at identifying voids in cosmological simulations, previous techniques based on web classification schemes usually perform a FOF-like algorithm over cells previously marked as voids according to some established criteria in order to construct bulk void regions [**references**]. Although this method has some success at classifying voids, percolation is completely inevitable, where the only way to reduce it is artificially decreasing the global volume fraction of void regions such that they do not merge significantly each other.

Once has been determined the reliability of the FA index for tracing the geometry of voids, our novel proposal here is rather using the FA field for classifying void regions. As was concluded in the previous subsection, the geometry of voids is completely traced by contours of the FA field, where central parts of voids and high density knot regions exhibit particularly low values of the FA index. Therefore, through a watershed transform all voids are classified, where each single void region corresponds to the basin of a local minimum of the FA field, where those local minimums are restricted to be embedded into a type-void cell in order to avoid degeneracy with knots.

5 PROPERTIES OF VOIDS

Once defined our method to classify bulk voids based upon web classification schemes of the cosmic web, we proceed to analyse some physical properties in order to compare their consistency with the geometry of voids as quantified by our method and by density-based schemes. Next, through the reduced inertia tensor we quantify the shape distribution of voids. Finally, we compute numerical radial profiles of density and peculiar velocity of bulk voids.

5.1 Statistics of halos in voids

One of the main challenges in observational void finding is the discrete nature of galaxy surveys

we calculate contours of discrete fields like the median mass and the local number of local dark matter halos and

, like the inertia values, the density and peculiar velocities profiles as calculated over the grid and profiles of number of halos.

5.2 Shape of voids

Quantifying the shape of voids is gaining importance due to cosmological tests such as the Alcock-Paczynski test [**Sutter et al 2012**], so we compute here the reduced inertia tensor through the next expression in order to determine shape distributions of bulk voids.

$$\tau_{ij} = \sum_l \frac{x_{l,i} x_{l,j}}{R_l^2} \tag{5}$$

where l is an index associated to each cell of the current region, i and j indexes run over each spatial direction and finally R_l is defined as $R_l^2 = x_{l,1}^2 + x_{l,2}^2 + x_{l,3}^2$. All positions are measured from the respective geometric center of each void.

The eigenvalues of the reduced inertia tensor, i.e. the principal moments of inertia, are used to quantify the shape of each bulk void. They are denoted as τ_1, τ_2 and τ_3 such that $\tau_1 \leqslant \tau_2 \leqslant \tau_3$. In Figure **??** we show the computed distributions for τ_1/τ_2 and τ_2/τ_3 for voids larger than 8 cells in order to avoid statistic fluctuations due to small regions. We rather calculate histograms for these ratio quantities instead of each single value in order to avoid using an arbitrary normalization. For both schemes, it can be noticed that the shape distribution is completely spread out, thereby indicating a non-preferred geometry of void regions, which is in agreement with the well established high anisotropy of matter flows associated to this type of region.

For a better quantification, we also perform a classification of the shape of voids by setting a threshold in the analysed ratio quantities. An anisotropic or tri-axial shape correspond to voids where $\tau_1/\tau_2 < 0.7$ and $\tau_2/\tau_3 < 0.7$, where there is not any symmetry among the principal directions. We find about $57.2\% \sim 61.0\%$ of total voids consistent with this shape, for the T-web and V-web respectively. A pancake or quasi-oblate shape is associated to voids where $\tau_1/\tau_2 < 0.7$ and $\tau_2/\tau_3 > 0.7$. We found $13.1\% \sim 17.9\%$ of consistent voids. Filamentary or quasi-prolate voids satisfy $\tau_1/\tau_2 > 0.7$ and $\tau_2/\tau_3 < 0.7$, with $25.4\% \sim 18.1\%$ of all voids. Finally, isotropic or quasi-spheric voids are found when $\tau_1/\tau_2 > 0.7$ and $\tau_2/\tau_3 > 0.7$, with $4.2\% \sim 3.1\%$ of total voids compatible with this shape. The threshold value of 0.7 adopted here for the ratios of the moments of inertia is just for illustrative purposes, where such distinction is rather fuzzy and continuous. However, the previous analysis allows us to conclude that voids are quite asymmetric structures.

5.3 Density profile of voids

Describing the density profiles of voids is quite important in order to compare and match simulation with observational surveys, allowing possible constrains for different cosmology models [**Hamaous, et.al 2014**]. Here, and taking into account the previous results, we rather use an ellipsoidal approximation to describe and fit the shape of bulk voids,

so we use the next ellipsoidal radial coordinate to describe density profiles.

$$r^2 = \frac{x^2}{\tau_1^2} + \frac{y^2}{\tau_2^2} + \frac{z^2}{\tau_3^2}, \quad 0 \leqslant r \leqslant 1 \tag{6}$$

where we take the principal moments of inertia $\{\tau_i\}$ as the lengths of the principal axes of the ellipsoid and each one of the cartesian coordinates as measured in the rotated frame of each void.

We use the same analytic density profile that [Hamaous, et.al 2014] to fit the numerical density profiles of our voids.

$$\delta_v(r) = \delta_c \frac{1 - (r/r_s)^\alpha}{1 + (r/r_v)^\beta} \tag{7}$$

6   CONCLUSIONS

ACKNOWLEDGMENTS

REFERENCES

Abazajian K., et al. (the SDSS Collaboration) 2003, AJ, 126, 2081

Basser P., 1995, NMR in Biomedical Imaging, 8, 333

Bertschinger E., 1985, ApJS, 58, 1

Beucher S., Lantuejoul C., 1979, in Proceedings International Workshop on Image Processing, CCETT/IRISA, Rennes, France

Beucher S., Meyer F., 1993, Mathematical Morphology in Image Processing. Marcel Deker, New York

Blumenthal G. R., da Costa L. N., Goldwirth D. S., Lecar M., Piran T., 1992, ApJ, 388, 234

Bond J. R., Kofman L., Pogosyan D., 1996, Nature, 380, 603

Brunino R., Trujillo I., Pearce F. R., Thomas P. A., 2007, MNRAS, 375, 184

Ceccarelli L., Padilla N. D., Valotto C., Lambas D. G., 2006, MNRAS, 373, 1440

Ceccarelli L., Paz D., Lares M., Padilla N., Lambas D. G., 2013, MNRAS, 434, 1435

Chincarini G., Rood H. J., 1975, Nature, 257, 294

Colberg J. M., Pearce F., et al. 2008, MNRAS, 387, 933

Colberg J. M., Sheth R. K., Diaferio A., Gao L., Yoshida N., 2005, MNRAS, 360, 216

Colless M., et al. (the 2dFGRS Team), 2001, MNRAS, 328, 1039

Colless M., et al. (the 2dFGRS Team), 2003, VizieR Online Data Catalog, 7226

Croton D. J., et al. 2004, MNRAS, 352, 828

Dubinski J., da Costa L. N., Goldwirth D. S., Lecar M., Piran T., 1993, ApJ, 410, 458

Einasto J., Joeveer M., Saar E., 1980a, MNRAS, 193, 353

Einasto J., Joeveer M., Saar E., 1980b, Nature, 283, 47

Forero-Romero J. E., Hoffman Y., Gottlöber S., Klypin A., Yepes G., 2009, MNRAS, 396, 1815

Foster C., Nelson L. A., 2009, ApJ, 699, 1252

Gottlöber S., Łokas E. L., Klypin A., Hoffman Y., 2003, MNRAS, 344, 715

Gregory S. A., Thompson L. A., 1978, ApJ, 222, 784

Hahn O., Porciani C., Carollo C. M., Dekel A., 2007, MNRAS, 375, 489

Hoffman Y., Metuki O., Yepes G., Gottlöber S., Forero-Romero J. E., Libeskind N. I., Knebe A., 2012, MNRAS, 425, 2049

Hoffman Y., Shaham J., 1982, ApJL, 262, L23

Hoyle F., Vogeley M. S., 2004, ApJ, 607, 751

Icke V., 1984, MNRAS, 206, 1P

Jarosik N., Bennett C. L., et al. 2011, ApJS, 192, 14

Kauffmann G., Fairall A. P., 1991, MNRAS, 248, 313

Kirshner R. P., Oemler Jr. A., Schechter P. L., Shectman S. A., 1981, ApJL, 248, L57

Kirshner R. P., Oemler Jr. A., Schechter P. L., Shectman S. A., 1987, ApJ, 314, 493

Klypin A., Gottlöber S., Kravtsov A. V., Khokhlov A. M., 1999, ApJ, 516, 530

Klypin A. A., Trujillo-Gomez S., Primack J., 2011, ApJ, 740, 102

Libeskind N. I., Hoffman Y., Forero-Romero J., Gottlöber S., Knebe A., Steinmetz M., Klypin A., 2013, MNRAS, 428, 2489

Martel H., Wasserman I., 1990, ApJ, 348, 1

Micheletti D., et al. 2014, ArXiv e-prints

Müller V., Arbabi-Bidgoli S., Einasto J., Tucker D., 2000, MNRAS, 318, 280

Nadathur S., Hotchkiss S., 2014, MNRAS, 440, 1248

Neyrinck M. C., 2008, MNRAS, 386, 2101

Neyrinck M. C., Falck B. L., Szalay A. S., 2013, ArXiv e-prints

Pan D. C., Vogeley M. S., Hoyle F., Choi Y.-Y., Park C., 2012, MNRAS, 421, 926

Patiri S. G., Betancort-Rijo J., Prada F., 2006, MNRAS, 368, 1132

Patiri S. G., Prada F., Holtzman J., Klypin A., Betancort-Rijo J., 2006, MNRAS, 372, 1710

Platen E., van de Weygaert R., Jones B. J. T., 2007, MNRAS, 380, 551

Plionis M., Basilakos S., 2002, MNRAS, 330, 399

Regos E., Geller M. J., 1991, ApJ, 377, 14

Ricciardelli E., Quilis V., Planelles S., 2013, MNRAS, 434, 1192

Riebe K., Partl A. M., Enke H., Forero-Romero J., Gottloeber S., Klypin A., Lemson G., Prada F., Primack J. R., Steinmetz M., Turchaninov V., 2011, ArXiv e-prints

Rojas R. R., Vogeley M. S., Hoyle F., Brinkmann J., 2005, ApJ, 624, 571

Schaap W. E., van de Weygaert R., 2000, A&A, 363, L29

Shandarin S., Feldman H. A., Heitmann K., Habib S., 2006, MNRAS, 367, 1629

Sutter P. M., Lavaux G., Hamaus N., Pisani A., Wandelt B. D., Warren M. S., Villaescusa-Navarro F., Zivick P., Mao Q., Thompson B. B., 2014, ArXiv e-prints

Sutter P. M., Lavaux G., Wandelt B. D., Weinberg D. H., 2012, ApJ, 761, 44

Sutter P. M., Lavaux G., Wandelt B. D., Weinberg D. H., Warren M. S., 2014, MNRAS, 438, 3177

Tikhonov A. V., 2006, Astronomy Letters, 32, 727

Tikhonov A. V., 2007, Astronomy Letters, 33, 499

van de Weygaert R., van Kampen E., 1993, MNRAS, 263, 481

von Benda-Beckmann A. M., Müller V., 2008, MNRAS, 384, 1189

York D. G., et al. (the SDSS Collaboration), 2000, AJ, 120,
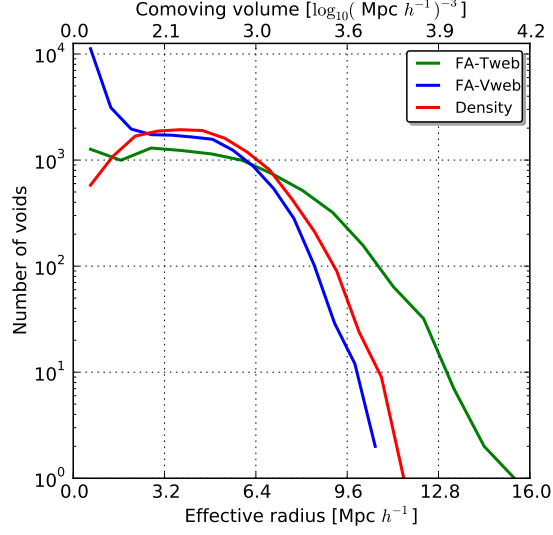 1579
Zel'dovich Y. B., 1970, A&A, 5, 84

Figure 4. Volume functions of voids catalogued by each used scheme. Left panel (watershed transform over the FA field of the T-web scheme). Central panel (over the FA field of the V-web scheme). Right panel (over the density field). Gray curves correspond to voids without boundary removal whereas black curves are associated to voids merged through boundary removal process. Dotted lines correspond to original continuous fields, while segmented lines correspond to fields with a 1st-order median filtering and continuous lines to a 2nd-order median filtering.
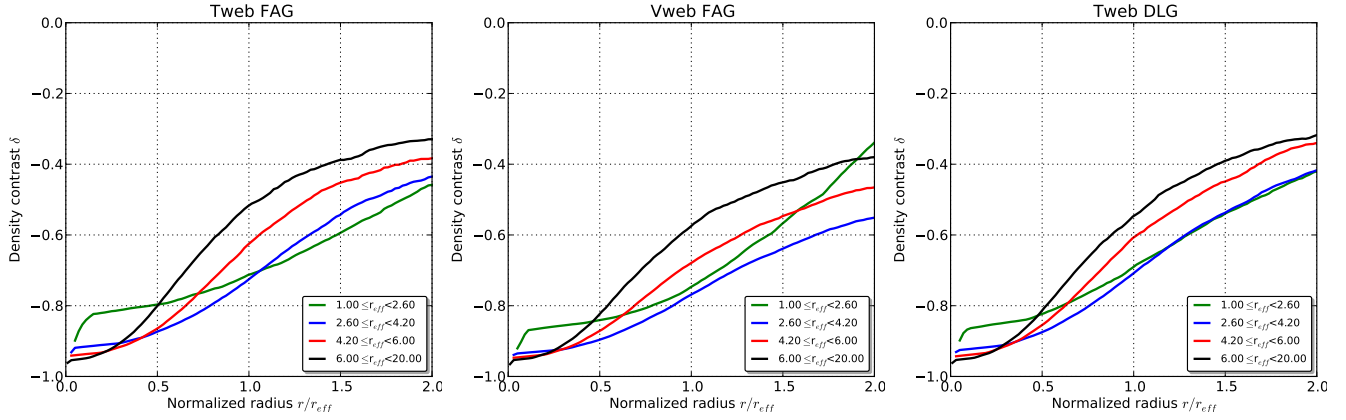

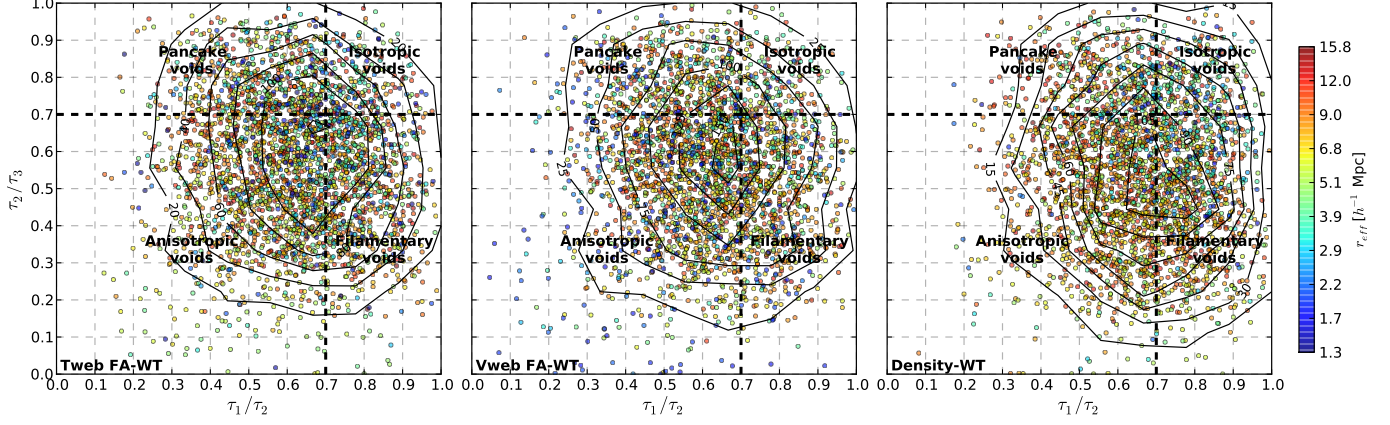**Figure 5.** Density profiles of voids for each finding scheme.

Figure 6. Volume functions of voids catalogued by each used scheme. Left panel (watershed transform over the FA field of the T-web scheme). Central panel (over the FA field of the V-web scheme). Right panel (over the density field). Gray curves correspond to voids without boundary removal whereas black curves are associated to voids merged through boundary removal process. Dotted lines correspond to original continuous fields, while segmented lines correspond to fields with a 1st-order median filtering and continuous lines to a 2nd-order median filtering.